

Dielectron production in pion-nucleon reactions at intermediate energies

A.P.Ierusalimov, G.I.Lykasov

JINR, Dubna, Moscow region, 141980, Russia

Abstract

Dielectron production in the πN interaction at not large energies is studied. The dominant contribution of the Δ -isobar creation in the intermediate state at incident pion momenta of about 0.3-0.4 GeV/c is shown. The experimental distributions over the angle and effective mass $M_{e^+e^-}$ of the e^+e^- pair are described satisfactorily. This stimulated us to present theoretical predictions for the $M_{e^+e^-}$ distribution in the process $\pi^- p \rightarrow n e^+ e^-$ at different incident momenta, which could be verified, for example, by the HADES experiments.

1. Introduction

Processes of meson electroproduction play an important role in the study of the structure and properties of matter, see, for example, the review in ref. [1] and references therein. The production of dileptons in hadron-hadron, hadron-nucleus and nucleus-nucleus reactions has been analyzed very intensively [2]-[8]. In these reactions, virtual photons, which materialize as e^+e^- pairs, carry unique information on the properties of matter and the reaction mechanism.

Inverse pion electroproduction (IPE), $\pi N \rightarrow e^+e^-N$, can provide information on the nucleon electromagnetic structure in the time-like region. An intense pion beam could allow to perform more detailed experiments on the IPE aimed at both extracting the hadron structure and carrying out a multipole analysis like in the case of photoproduction and electroproduction, see for example [9] and references therein.

2. General formalism

We analyze the reaction $\pi N \rightarrow \gamma^* N \rightarrow e^+e^-N$ within the unified model. This means that in the one-photon approximation, owing to T -invariance, three reactions $\gamma N \rightarrow \pi N, eN \rightarrow e\pi N$ and $\pi N \rightarrow e^+e^-N$ are related to the process $\gamma^* N \leftrightarrow \pi N$ by the hadron current $J_\mu(s, t, m_\gamma^2)$, where $m_\gamma^2 = 0, > 0$ and $m_\gamma^2 < 0$ correspond to pion photoproduction, electroproduction and inverse pion electroproduction (IPE),

respectively [10, 4]. For the IPE the S -matrix in the one-photon approximation reads as

$$S_{fi} = \delta_{fi} + (2\pi)^4 i\delta^{(4)}(p + q\pi - q - p') \frac{m}{\sqrt{2q_{\pi 0} p_0 q_0 p'_0}} \epsilon^\mu J_\mu(s, t, m_{\gamma^*}^2), \quad (1)$$

where ϵ^μ is the electromagnetic current and photon propagator

$$\epsilon^\mu = \bar{u}(k_2) \gamma^\mu u(k_1) e/q^2 \quad (2)$$

According to [10], the current J_μ can also be presented in the following form:

$$J_\mu = \sum_{i=1}^8 B_i(s, t, u, q^2) N_\mu^i, \quad (3)$$

where the functions N_μ^i related to the Dirac γ_μ matrices are presented in the Appendix, see also [10]. Inserting functions N_μ^i into Eq. 3 one can obtain the following form for the current J_μ :

$$J_\mu = \gamma_5 [G_1 P_\mu + G_2 q_{\pi\mu} + G_3 q_\mu + G_4 \gamma_\mu + G_5 \hat{q} P_\mu + G_6 \hat{q} q_{\pi\mu} + G_7 \hat{q} q_\mu + G_8 \hat{q} \gamma_\mu], \quad (4)$$

where $\hat{q} = \tilde{q}^\nu \gamma_\nu$, $\tilde{q} = q/|q|$ is the unit photon four-momentum ;

$$\begin{aligned} B_1 &= -iG_8, \quad B_2 = 2iG_1, \quad B_3 = 2iG_2, \quad B_4 = 2i(G_3 + 2G_8), \\ B_5 &= G_4, \quad B_6 = G_5, \quad B_7 = G_7, \quad B_8 = G_6. \end{aligned} \quad (5)$$

Using the current conservation law

$$q^\mu J_\mu = 0, \quad (6)$$

we actually obtain 6 independent functions instead of 8, see [10]. The forms for functions G_i depending on the Mandelstam relativistic invariants s, t and u are obtained calculating the Feynman graphs presented in Figs. (1,2).

On the other hand, applying the current conservation law given by Eq.(6) one can obtain the following form for $\epsilon^\mu J_\mu$, as a sum of six independent functions $A_i(s, t, u, q^2)$:

$$\epsilon^\mu J_\mu = \sum_{i=1}^6 A_i(s, t, u, q^2) M_\mu^i \quad (7)$$

where the functions M_μ^i are presented in [10] and $A_i(s, t, u, q^2)$ are related to the functions $B_i(s, t, u, q^2)$ entering into Eq.(7),

$$\begin{aligned} A_1 &= B_1 - mB_6, \quad A_2 = \frac{2B_2}{t - \mu^2}, \quad A_3 = -B_8, \quad A_4 = -\frac{1}{2}B_6, \\ A_5 &= \frac{1}{q \cdot q_\pi} (B_1 + 2B_4 - \frac{2P \cdot q}{t - \mu^2}), \quad A_6 = B_7, \end{aligned} \quad (8)$$

The current J_μ can also be presented in terms of Pauli matrices [2, 10, 11], see Appendix.

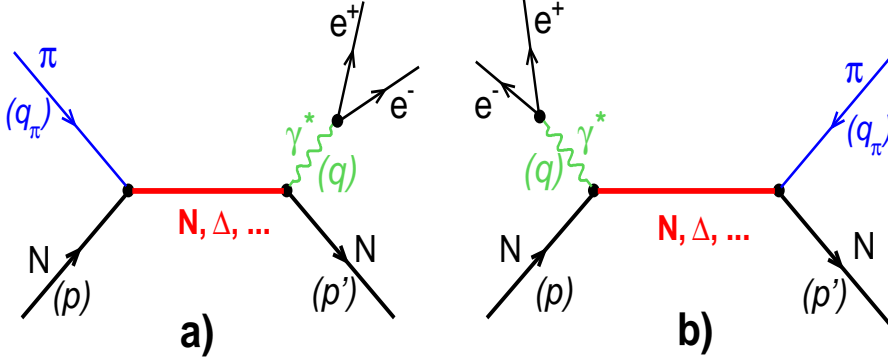


Figure 1: The one-nucleon or one-nucleon resonance exchange graph in the s -channel of the IPE $\pi N \rightarrow \gamma N \rightarrow e^+e^-N$ process.

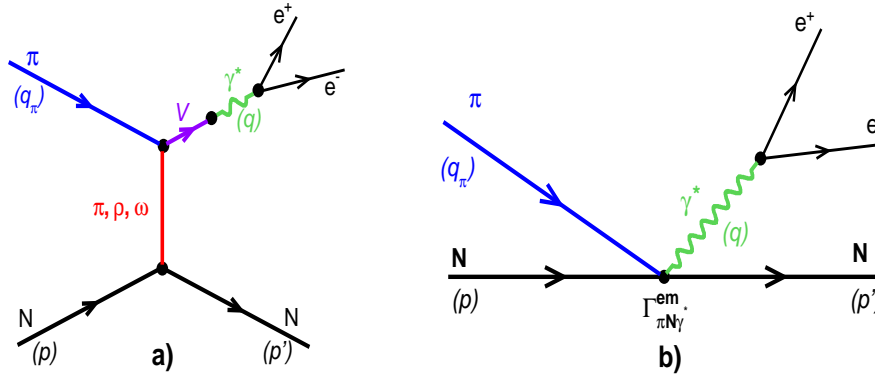


Figure 2: The one-meson exchange graph in the t -channel (a) and the electromagnetic contact term (b) for the IPE.

3. One-nucleon exchange graph

• s -channel one-nucleon exchange graph

Calculating the one-nucleon exchange Feynman graph in the s -channel (Fig.1a), the so-called Born-term, we use the effective meson-NN Lagrangian in the form (see [12, 7])

$$\mathcal{L}_{NN\pi} = -\frac{g_{NN\pi}}{2m_N} \bar{\Psi}_N \gamma_5 \gamma_\mu \tau \cdot (\partial^\mu \Phi_\pi) \Psi_N, \quad (9)$$

where Ψ_N is the spinor for a nucleon and Φ_π is the pion field. We use the monopole form factor in this interaction vertex

$$F_\pi^{NN} = \frac{\Lambda_\pi^2}{\Lambda_\pi^2 + q^2}, \quad (10)$$

where Λ is the cut-off parameter. The usual nucleon propagator is used

$$S_N^{(s)}(p_N) = \frac{\not{p}_N + m_N}{p_N^2 - m_N^2} = \frac{\not{p}' + \not{q} + m_N}{s - m_N^2} \equiv \frac{\not{p} + \not{q}_\pi + m_N}{s - m_N^2}, \quad (11)$$

where $\not{p}_N = p_N^\mu \cdot \gamma_\mu$, $p_N = p' + q = q_\pi + p$ is the four-momentum of the exchanged nucleon, $p_N^2 = s = (p + p_\pi)^2 = (p' + q)^2$, m_N is the nucleon mass, γ_μ is the Dirac matrix.

The general form for the effective Lagrangian for the nucleonic bremsstrahlung process $NN\gamma$ reads as

$$\mathcal{L}_{NN\gamma} = -e\bar{\Psi}_N \Gamma_\mu^{NN\gamma} A^\mu \Psi_N, \quad (12)$$

where A^μ is the electromagnetic field, the half-off-shell nucleon-photon vertex $\Gamma_\mu^{NN\gamma}$ is [7]

$$\Gamma_\mu^{NN\gamma} = -ie \sum_{s=\pm} (F_1 \gamma_\mu + F_2 \Sigma_\mu + F_3 q_\mu) \Lambda_s, \quad (13)$$

where $\Lambda_\pm = (\pm \not{p} + W)/W$ are the projection operators for the off-shell nucleon of mass $W = \sqrt{p^2}$ and $\Sigma_\mu = i\sigma_{\mu\nu} q^\nu / (2m)$. Here we use the on-shell form factors for the $NN\gamma$ vertex and assume that $F_1^+ = F_1^- = F_1$, $F_2^+ = F_2^- = F_2$ and $F_3^+ = F_3^- = 0$, as it was suggested in [7, 13, 14]. This assumption can be rather applicable at not large values of the initial pion. We will demonstrate this for a pion momentum of about 0.3 GeV/c

• *u*-channel one-nucleon exchange graph

For the one nucleon-exchange graph in the *u*-channel (Fig.1b) the propagator reads

$$S_N^{(u)}(p_N) = \frac{\not{p}' - \not{q} + m_N}{u - m_N^2} \equiv \frac{\not{p}' - \not{q}_\pi + m_N}{u - m_N^2}, \quad (14)$$

where $u = (q_\pi - p')^2 = (p - q)^2$. We should also substitute the four-momenta q and q_π by $-q$ and $-q_\pi$ in all the vertices of this graph.

4. Δ -isobar exchange graph

In calculating the Δ -isobar exchange graphs in the *s*- and *u*-channels we use the same procedure as in [3, 7, 8]. In particular, the Δ -nucleon-photon vertex is

$$\Gamma_{\Delta N\gamma}^{\mu\nu} = -i \frac{e}{2m} \left\{ g_1(q^2) \gamma_\lambda + \frac{g_2(q^2)}{2m} p_\lambda^\Delta + \frac{g_3(q^2)}{2m} q_\lambda \right\} (-q^\nu g^{\mu\lambda} + q^\mu g^{\nu\lambda}), \quad (15)$$

where g_1, g_2, g_3 are the form factors used in the same monopole form and the coupling constants are like in [7]. We use the following effective Δ - nucleon - meson Lagrangian [7, 15]:

$$\mathcal{L}_{\Delta N\pi} = \frac{g_{\Delta N\pi}}{m u_\pi} \bar{\Psi}_\mu^\Delta \gamma_5 \partial^\mu \Phi_\pi \Psi_N + H.c., \quad (16)$$

where Ψ_μ^Δ is the vector spinor for the Δ -isobar. The propagator for the Δ -isobar reads

$$S_\Delta^{\mu\nu}(p_\Delta) = -\frac{i(\not{p}_\Delta + m_\Delta)}{p_\Delta^2 - (m_\Delta - i(\Gamma_\Delta)/2)^2} (g^{\mu\nu} - \frac{1}{3} \gamma^\mu \gamma^\nu - \frac{2}{3m_\Delta^2} p_\Delta^\mu p_\Delta^\nu + \frac{1}{3m_\Delta} (p_\Delta^\mu \gamma^\nu - p_\Delta^\nu \gamma^\mu)) \quad (17)$$

where p_Δ and M_Δ are the four-momentum and the mass of the Δ isobar created in the intermediate state (Figs.1(a,b)) and the partial width of the off-shell Δ -isobar $\Gamma_\Delta \equiv \Gamma_{\Delta \rightarrow \pi N}$ is [7, 16, 17, 18]

$$\Gamma_\Delta(M) = \Gamma_0 \left(\frac{k^*(M)}{k^*(M_\Delta)} \right)^3 \frac{M_\Delta}{M} \left(\frac{\beta^2 + (k^*(M_\Delta))^2}{\beta^2 + (k^*(M))^2} \right)^2 . \quad (18)$$

Here $\Gamma_0 = 0.12 GeV$ is the bar width of Δ , β is the parameter, we assumed $\beta^2 = 0.25(GeV/c)^2$ as in [7], k^* is the pion momentum in the $\pi - N$ c.m.s. and $k^*(M) = \lambda^{1/2}(M^2, \mu_\pi^2, m^2)/2M$

5. One-meson exchange in t -channel

Calculating the Feynman graphs corresponding to the one-meson exchange in the t -channel, Fig.2a, we only included the one-pion exchange so as to analyze the IPE processes at intermediate energies less than 0.5-0.6 GeV when the vector meson exchange graphs contribute insignificantly and can be neglected. Moreover, note that the G -parity arguments forbid $\omega\pi\pi$ and $A_1\pi\pi$ vertices, so the pion current diagram (Fig.2a) only contributes in the case of isovector currents. The $NN\pi$ Lagrangian was taken in the form given by eq.(9), whereas the Lagrangian of the $\rho\pi\pi$ interaction was taken in the following form [20]:

$$\mathcal{L}_{\rho\pi\pi} = g_\rho \epsilon_{jlm} \Phi_{\rho,\mu}^j \Phi_\pi^l \partial_\mu \Phi_\pi^m , \quad (19)$$

where Φ_ρ and Φ_π are the ρ -meson and pion fields respectively, ϵ_{jlm} is the fully antisymmetric unit tensor. The coupling constant $g_\rho \equiv g_{\rho\pi\pi}$ was found from the $SU(3)$ relation [20] $2g_{\rho NN} = g_\rho$, whereas the coupling constant $g_{\rho NN}$ was taken from [21]. The Lagrangian corresponding to the $\rho\gamma$ vertex (Fig.2a) was taken in the following form [8]:

$$\mathcal{L}_{\rho\gamma}^{em} = -\frac{e}{2f_{\rho\gamma}} \mathcal{F}^{\mu\nu} \mathcal{G}_{\nu\mu}^\rho , \quad (20)$$

where $\mathcal{F}^{\mu\nu}$ and $\mathcal{G}^{\nu\mu}$ are the strength tensors for the photon and ρ -meson fields. For the ρ -meson propagator $S_\rho^{\mu\nu}$ of Fig.2a we obtained the same form as in [7],

$$S_\rho^{\mu\nu}(q^2) = -i \left(\frac{g^{\mu\nu} - q^\mu q^\nu / q^2}{q^2 - m_\rho^2} \right) , \quad (21)$$

where m_ρ is the ρ -meson mass. The pion propagator (Fig.2a) reads

$$S_\pi(t) = \frac{i}{t - \mu_\pi^2} , \quad (22)$$

where $t = (q_\pi - q)^2$.

6. Electromagnetic contact term

When the pseudovector πNN interaction given by Eq.(9) is used then the contact electromagnetic diagram (Fig.2b) should be included. The electromagnetic contact terms, e.g., the vertices with four lines as in Fig.2b, [22, 8, 23] correspond to the following interaction Lagrangian:

$$\mathcal{L}_{NN\pi\gamma} = - \frac{\hat{e} f_{NN\pi}}{\mu_\pi} \bar{\Psi}_N \gamma_5 \gamma_\mu A_\mu (\tau \cdot \Phi_\pi) \Psi_N , \quad (23)$$

where \hat{e} is the charge operator of the pion.

7. Amplitude and cross section

In the one-photon approximation the dilepton production in the IPE process is considered as a decay of the virtual photon produced in strong and electromagnetic $\pi - N$ interactions. These processes and the similar $NN \rightarrow \gamma^* NN \rightarrow e^+ e^- NN$ reactions have already been investigated, see for example [10]-[8], where all the details to obtain the forms for the amplitude and differential cross sections are presented. The general expression for the IPE relativistic invariant amplitude squared reads

$$|\mathcal{T}|^2 = W_{\mu\nu} \frac{e^2}{q^2} l^{\nu\mu} , \quad (24)$$

where e is the electron charge, $q^2 = m_{\gamma^*}^2 = (k_1 + k_2)^2$, q is the four-Momentum of the virtual time-like photon decaying into e^+ and e^- with the four-Momenta K_1 and k_2 respectively; $W_{\mu\nu} = \sum_{spins} J_\mu J_\nu^+$ is the hadronic tensor, whereas $l^{\nu\mu}$ is the leptonic tensor.

$$l_{\nu\mu} = 4(k_{1\nu} k_{2\mu} + k_{1\mu} k_{2\nu} - g_{\nu\mu} (k_1 \cdot k_2)) \quad (25)$$

where k_1 and k_2 are the four-momenta of the outgoing electron and positron, respectively. Following the procedure to get the differential cross section presented in [8] one can obtain the following forms for the effective mass distribution $d\sigma/dM_{e^+e^-}$ of the e^+e^- pair and the angular distribution $d\sigma/d\cos\theta_{\gamma^*}^*$ of the virtual γ^* in the $\pi - N$ c.m.s.:

$$\frac{d\sigma}{dM_{e^+e^-}} = \frac{\alpha_{em}^2}{12\pi M_{e^+e^-} s \lambda^{1/2}(s, \mu_\pi m^2)} \int_{t^-}^{t^+} \frac{\lambda^{1/2}(s, q^2, m^2)}{s} \sum_{spins} J_\mu J_\nu^+ dt ; \quad (26)$$

$$\frac{d\sigma}{d\cos\theta_{\gamma^*}^*} = \frac{\alpha_{em}^2}{48\pi s \lambda^{1/2}(s, \mu_\pi m^2)} \int \frac{\lambda^{1/2}(s, q^2, m^2)}{q^2} \sum_{spins} J_\mu J_\nu^+ dq^2 , \quad (27)$$

where $\alpha_{em} = e^2/4\pi = 1/137$; $\lambda(x^2, y^2, z^2) = (x^2 - (y + z)^2) = (x^2 - (y - z)^2)$.

8. Dalitz decay of Δ resonance

The effective mass distribution of the e^+e^- pair produced in the $\pi - N$ reaction at an energy corresponding to the Δ isobar creation in the intermediate state can be estimated applying the simple Breit-Wigner approximation and the Dalitz decay of the Δ isobar, [18]

$$\frac{d\sigma_{\pi N}^{Br.W.}}{dM_{e^+e^-}} = \frac{1}{3} \frac{4\pi}{(k^*)^2} \frac{M_\Delta^2 \Gamma_\Delta}{(M_\Delta^2 - s - iM_\Delta \Gamma_{tot})^2} \frac{d\Gamma_{\Delta \rightarrow \gamma^* N \rightarrow e^+e^- N}}{dM_{e^+e^-}}, \quad (28)$$

where Γ_Δ is given by Eq.(18) and

$$\frac{d\Gamma_{\Delta \rightarrow \gamma^* N \rightarrow e^+e^- N}}{dM_{e^+e^-}} = \frac{2\alpha_{em}}{3\pi M_{e^+e^-}} \sqrt{1 - \frac{4\mu_e^2}{M_{e^+e^-}^2}} \left(1 + \frac{2\mu_e^2}{M_{e^+e^-}^2}\right) \Gamma_{\Delta \rightarrow \gamma^* N}; \quad (29)$$

$$\Gamma_{\Delta \rightarrow \gamma^* N} = \frac{p_\Delta^*}{8\pi m_\Delta^2} |\mathcal{M}_{\Delta \rightarrow \gamma^* N}|^2. \quad (30)$$

Here p_Δ^* is the momentum in the $\gamma^* N$ c.m.s. and the matrix element squared reads

$$|\mathcal{M}_{\Delta \rightarrow \gamma^* N}|^2 = e^2 G_M^2 \frac{(m_\Delta + m)^2 ((m_\Delta - m)^2 - M_{e^+e^-}^2)}{4m^2 ((m_\Delta + m)^2 - M_{e^+e^-}^2)} (7m_\Delta^4 + 14m_\Delta^2 M_{e^+e^-}^2 + 3M_{e^+e^-}^4 + 8m_\Delta^3 m + 2m_\Delta^2 m^2 + 6M_{e^+e^-}^2 m^2 + 3m^4). \quad (31)$$

The angular distribution of γ^* is presented in [18].

9. Results and discussion

We have calculated the distributions of e^+e^- pairs as functions of the dielectron effective mass $M_{e^+e^-}$ and of $\cos\theta_{\gamma^*}$, respectively, see Eqs. (26,27), adding incoherently the Dalitz decay of the Δ resonance. In Fig. 3 the angular distribution $d\sigma/d\cos\theta_{\gamma^*}$, where θ_{γ^*} is the angle of the virtual photon γ^* , is presented. This distribution was summed over q^2 in the interval $0.046(GeV/c)^2 \geq q^2 \leq 0.065(GeV/c)^2$, according to the experimental data [24]. The solid curve corresponds to our calculations, e.g., the coherent sum of the one-nucleon and Δ -exchange graphs with the positive phase sign of the second graph. The experimental data are taken from [24]. It is seen from this figure that our total calculation results in a more or less isotropic distribution and provides the qualitative description of the data, which have big error bars.

In Fig. 4 the invariant mass distribution for dielectrons $d\sigma/dM_{e^+e^-}^2$ produced in the reaction $\pi^- p \rightarrow e^+e^- n$ is presented. The histogram is the experimental data in arbitrary units [25]. The solid curve is our total calculation, e.g. the coherent sum of all the graphs of Figs.(1,2). The dash-dotted curve is the contribution of Δ -exchange diagrams of Fig.1, while the dotted curve corresponds to the calculation using the Breit-Wigner form for the spectrum given by Eq.(28) including the Dalitz decay

of Δ . The long dashed line corresponds to the incoherent sum of the one-nucleon and Δ isobar exchange diagrams. The Dalitz decay of resonances was calculated, according to [18], see also [26].

In Fig. 5 the invariant mass distribution for dielectrons, $d\sigma/dM_{e^+e^-}$, produced in reaction $\pi^- p \rightarrow e^+ e^- n$ at different pion momenta. The solid, dashed, dash-dotted and dotted curves correspond to calculations at the initial pion momentum about 100 MeV/c, 300 MeV/c, 400 MeV/c and 700 MeV/c respectively. The thick lines correspond to our calculations without any form factors $F(q^2)$ (or $F(t)$), while the thin curves correspond to inclusion of the form factors in the vertices of diagrams in Figs. (1,2).

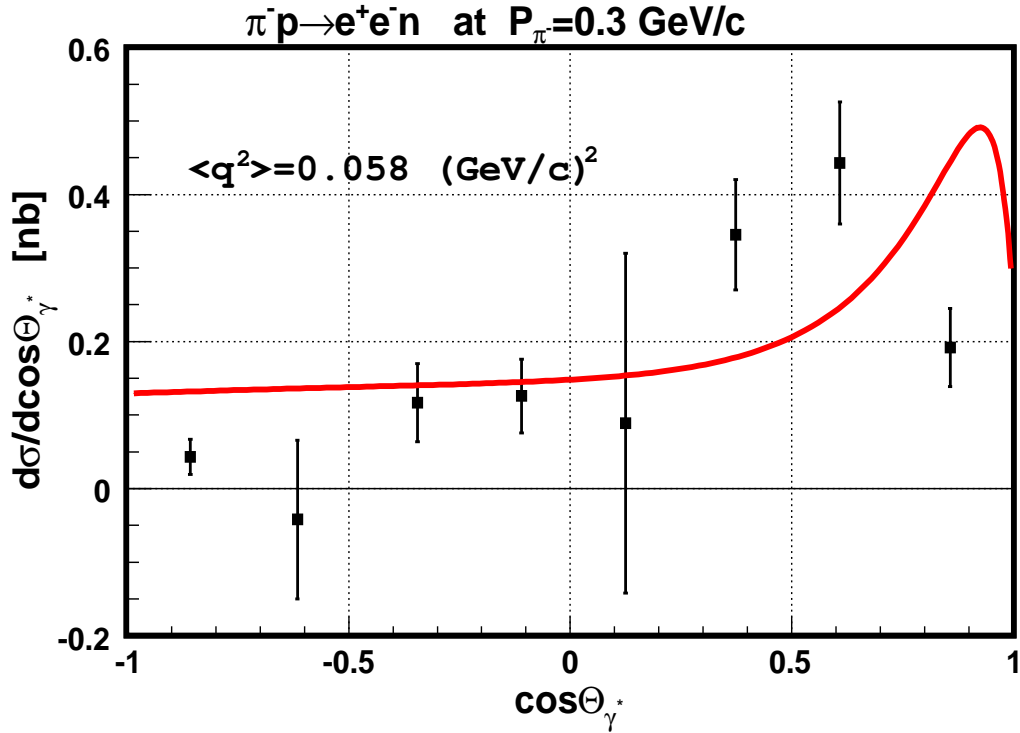


Figure 3: Angular distribution $d\sigma/d\cos\theta_{\gamma^*}$, where θ_{γ^*} is the angle of the virtual photon γ^* . The solid curve corresponds to our calculations. The experimental data are taken from [24].

Let us note that our calculations were performed using the Feynmann diagrams of Figs. (1,2), which result in the main contribution to the observables presented in Figs. (4,5), see for example, [19]. In our calculations we neglected the contributions of processes $\pi^- p \rightarrow \pi^0 p \rightarrow e^+ e^- \gamma p$, $\pi^- p \rightarrow \eta^0 p$ and $\pi^- p \rightarrow \rho^0 p$ with subsequent decays ($\eta^0 \rightarrow e^+ e^- \gamma$ and $\rho^0 \rightarrow e^+ e^-$ respectively) because they can be significant at initial momenta above 600-700 MeV/c and high dielectron effective masses $M_{e^+e^-} \geq 0.5 \text{ GeV}/c^2$, as it has been shown in [27, 28].

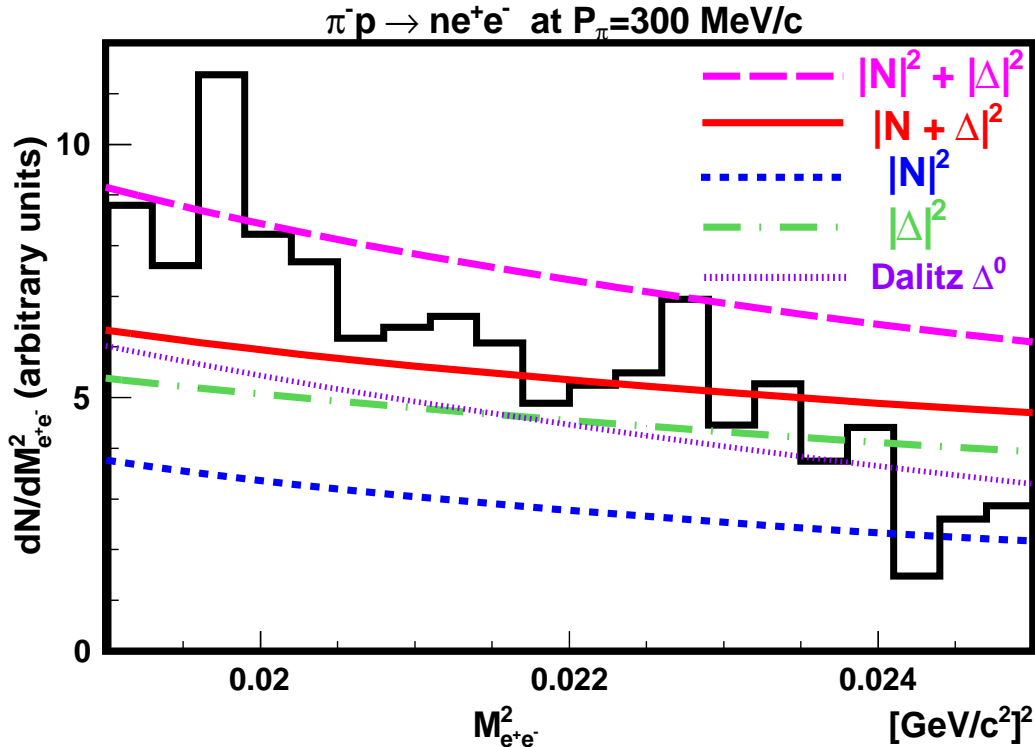


Figure 4: Invariant mass distribution for dielectrons, $d\sigma/dM_{e^+e^-}^2$, produced in the reaction $\pi^- p \rightarrow e^+e^- n$. The histogram presents the experimental data in arbitrary units [25]. Contributions of the Dalitz decay, the one-nucleon exchange and the Δ -isobar exchange correspond to the dotted, short dashed and dash-dotted curves respectively. The solid curve is our calculation of the coherent sum of all diagrams of Figs. (1,2), the dashed line corresponds to the incoherent sum of the one-nucleon and Δ -exchange contributions.

10. Conclusion

In this paper we have analyzed inverse pion electroproduction (IPE) processes $\pi N \rightarrow e^+e^- N$ at intermediate energies within the Feynman graph formalism. The dominant contribution of the Δ -isobar exchange graph in the s -channel to the effective mass spectrum of e^+e^- pairs produced at incident pion momenta of about 0.3-0.4 GeV/c is shown, while at higher momenta it decreases. At higher momenta the contributions of diagrams with another baryon-exchange in the s -channel and with a vector meson-exchange in the t -channel are considerable. We show that careful calculations of the Feynman graphs with account of their interference provides correct results for the observables which may differ from the results of approximate calculations involving only bremsstrahlung of the nucleon and the Dalitz decay of baryon resonances in the intermediate state. The existing experimental information on these processes is very poor. Therefore we present predictions for the $M_{e^+e^-}$

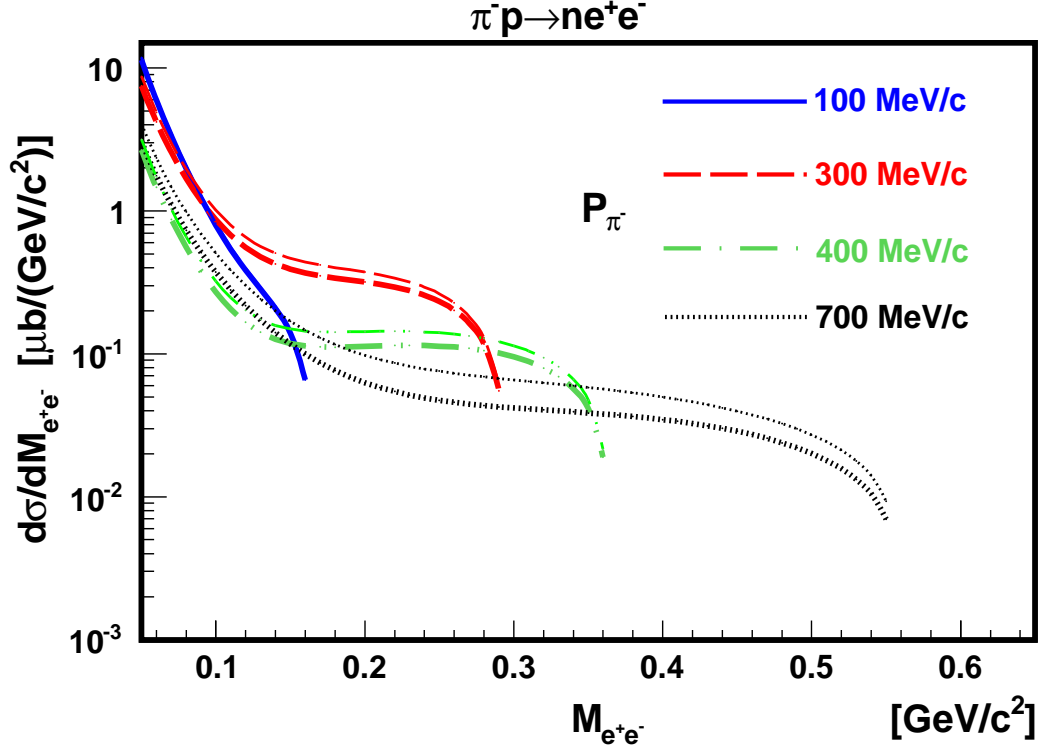


Figure 5: Invariant mass distribution for dielectrons, $d\sigma/dM_{e^+e^-}$, produced in reaction $\pi^-p \rightarrow e^+e^-n$ at different pion momenta. The thick curves correspond to calculations without any form factors $F(q^2)$ or $F(t)$, while the thin lines correspond to inclusion of the form factors in the vertices of diagrams in Figs. (1,2).

spectrum and the angular distribution of the virtual photon decaying into e^+e^- in the IPE reactions at incident momenta less than 1.GeV/c. This can be verified by future HADES experiments with pion beams. We will extend this approach to analyze inelastic $\pi p \rightarrow e^+e^-X$ reactions at HADES energies.

Acknowledgements. We are grateful to T.D.Blokhintseva, T.Galatyuk, B.Friman, G.Pontecorvo, R.Holzman, S.Kamalov, V.P. Ladygin, U.Mosel, B.Ramstein, A.Rustamov, P.Salabura, J.Stroth, V.Shklyar, Yu.Surovtsev for very useful discussions.

11. Appendix

$$\begin{aligned}
 N_1^\mu &= i\gamma_5\gamma^\mu\hat{q} ; N_2^\mu = 2i\gamma_5P^\mu ; N_3^\mu = 2i\gamma_5q_\pi^\mu ; N_4^\mu = 2i\gamma_5q^\mu ; \\
 N_5^\mu &= \gamma_5\gamma^\mu ; N_6^\mu = \gamma_5\hat{q}P^\mu ; N_7^\mu = \gamma_5\hat{q}q^\mu ; N_8^\mu = \gamma_5\hat{q}q_\pi^\mu
 \end{aligned}
 \tag{32}$$

$$\mathbf{J} = \frac{4\pi\sqrt{s}}{m} [i\tilde{\sigma}F_1 + \sigma \cdot \hat{\mathbf{q}}_\pi(\sigma \times \hat{\mathbf{q}})F_2 + i\tilde{\mathbf{q}}_\pi(\sigma \cdot \hat{\mathbf{q}})F_3 + i\hat{\mathbf{q}}_\pi(\sigma \cdot \hat{\mathbf{q}}_\pi)F_4 + i\hat{\mathbf{q}}(\sigma \cdot \hat{\mathbf{q}})F_6] , \tag{33}$$

where $\tilde{\sigma} = \sigma - \hat{\mathbf{q}}(\sigma \cdot \hat{\mathbf{q}}_\pi)$ and $\tilde{\mathbf{q}}_\pi = \hat{\mathbf{q}}_\pi - \hat{\mathbf{q}}(\hat{\mathbf{q}}_\pi \cdot \hat{\mathbf{q}})$. The J^0 component of the current J^μ can be obtained from the current conservation law given by Eq.(6)

$$J^0 = \frac{4\pi\sqrt{s}}{m} i[(\sigma \cdot \hat{\mathbf{q}}_\pi)F_7 + (\sigma \cdot \hat{\mathbf{q}})F_8] = \frac{\mathbf{q} \cdot \mathbf{J}}{q^0} . \quad (34)$$

Functions F_7, F_8 are related to F_5, F_6 [10, 11].

$$|\mathbf{q}| F_5 = q^0 F_8 ; \quad |\mathbf{q}| F_6 = q^0 F_7 \quad (35)$$

and functions $F_i, i = 1 - 6$ can be obtained calculating the Feynmann graphs of Figs. (1,2).

References

- [1] E.Amaldi, S.Fubini, and G.Furlan, *Electroproduction at Low Energy and Hadron Form Factors*, Springer Tracts in Modern Physics **83** (Springer, Berlin, 1979).
- [2] T.D.Blokhintseva, Yu.S.Surovtsev and M.Nagy, Acta Phys.Slovaca **49**, 351 (1999).
- [3] G.I.Smirnov, N.M.Shumeiko, Yaf, **17**, 1266 (1973).
- [4] Yu.S.Surovtsev, T.D.Blokhintseva, P.Bydzôvsky, M.Nagy, Phys.Rev. **C71**, 055205 (2005).
- [5] M.F.M.Lutz, B.Friman, and M.Soyeur, Nucl.Phys. **A713**, 97 (2003).
- [6] E.L.Bratkovskaya, W.Cassing, and U.Mosel, Nucl.Phys. **A686**, 568(2001).
- [7] R.Shyam and U.Mosel, Phys.Rev. **C67**, 065202 (2003); **C79**, 035203 (2009).
- [8] L.P.Kaptari and B.Kaempfer, Nucl.Phys., **A764**, 338 (2006); *ibid* nucl-th/0903.2466 (2009).
- [9] D. Drechsel, O. Hanstein, S.S. Kamalov and L. Tiator, Nucl. Phys. **A645**, 145 (1999).
- [10] F.A.Berends, A.Dannache and D.L.Weaver, Nucl.Phys.B **14**, 1 (1967).
- [11] D.Drechsel and L.Tiator, J.Phys.G:Nucl.Part.Phys., **18**,449 (1992).
- [12] T.Ericson and W.Weise, *Pions and Nuclei* (Clarendon, Oxford,1988).
- [13] M.Schaefer. H.C.Doenges, A.Engel and U.Mosel, Nucl.Phys., **A686**, 568 (2001).
- [14] K.Haglin, J.Kapusta and C.Gale, Phys.Lett., **B224**, 433 (1989).

- [15] T.Feuster and U.Mosel, Nucl.Phys. **A612**, 375 (1997); Phys.Rev. **C58**, 457 (1998); *ibid* **59**, 460 (1999).
- [16] Gy.Wolf, et al., Nucl.Phys., **A517**, 615 (1990).
- [17] S.Teis, et al., Z.Phys., **A356**, 421 (1997).
- [18] M.A.Kagarlis, GSI Report, **03** (2000);
I. Frohlich, et al., PoS ACAT, 076 (2007). [arXiv:0708.2382 [nucl-ex]].
- [19] V.N.Gribov, Sov.J.Nucl.Phys., **8**, 280 (1967).
- [20] I.S.Towner, Phys.Rep., **155**, 263 (1987).
- [21] R.Machleidt, K.Holinde and Ch.Elster, Phys.Rep., **149**, 1 91987).
- [22] N.M.Kroll, M.A.Ruderman, Phys.Rev. **93**, 233 (1954).
- [23] L.E.Marcucci, D.O.Riska, R.Schiavilla, Phys.Rev. **C58**, 3069 (1998).
- [24] S.Ph.Berezhnev, et.al., Sov.J.Nucl.Phys.,**24**, 591 (1976).
- [25] C.M.Hoffman, et al., Phys.Rev., **D28**, 660 (1983).
- [26] E.L.Bratkovskaya, W.Cassing, Nucl.Phys.**A807**, 214 (2008).
- [27] A.P.Jerusalimov, et al., Eur.Phys.J. A, **51**, 83 (2015).
- [28] A.P.Jerusalimov, G.I. Lykasov, arXiv:1704.00311 [nucl-th].